

# Proton widths of the low-lying $^{16}\text{F}$ states from the $^{15}\text{N}(^7\text{Li}, ^6\text{Li})^{16}\text{N}$ reaction

Z. D. Wu,<sup>1,2</sup> B. Guo,<sup>1,\*</sup> Z. H. Li,<sup>1</sup> Y. J. Li,<sup>1</sup> J. Su,<sup>1</sup> D. Y. Pang,<sup>3,4</sup> S. Q. Yan,<sup>1</sup>  
E. T. Li,<sup>5</sup> X. X. Bai,<sup>1</sup> X. C. Du,<sup>1</sup> Q. W. Fan,<sup>1</sup> L. Gan,<sup>1</sup> J. J. He,<sup>6</sup> S. J. Jin,<sup>1</sup>  
L. Jing,<sup>1</sup> L. Li,<sup>6</sup> Z. C. Li,<sup>1</sup> G. Lian,<sup>1</sup> J. C. Liu,<sup>1</sup> Y. P. Shen,<sup>1</sup> Y. B. Wang,<sup>1</sup> X.  
Q. Yu,<sup>6</sup> S. Zeng,<sup>1</sup> D. H. Zhang,<sup>2</sup> L. Y. Zhang,<sup>6</sup> W. J. Zhang,<sup>1</sup> and W. P. Liu<sup>1</sup>

<sup>1</sup>*China Institute of Atomic Energy,  
P.O. Box 275(10), Beijing 102413, China*

<sup>2</sup>*Institute of Modern Physics, Shanxi Normal University, Linfen 041004, China*

<sup>3</sup>*School of Physics and Nuclear Energy Engineering,  
Beihang University, Beijing 100191, China*

<sup>4</sup>*International Research Center for Nuclei and Particles in the Cosmos,  
Beihang University, Beijing 100191, China*

<sup>5</sup>*College of Physics Science and Technology,  
Shenzhen University, Shenzhen 518060, China*

<sup>6</sup>*Institute of Modern Physics, Chinese Academy of Sciences (CAS), Lanzhou 730000, China*

(Dated: April 30, 2022)

## Abstract

All the  $^{16}\text{F}$  levels are unbound by proton emission. To date the four low-lying  $^{16}\text{F}$  levels below 1 MeV have been experimentally identified with well established spin-parity values and excitation energies with an accuracy of 4-6 keV. However, there are still considerable discrepancies for their level widths. The present work aims to explore these level widths through an independent method. The angular distributions of the  $^{15}\text{N}(^7\text{Li}, ^6\text{Li})^{16}\text{N}$  reaction leading to the first four states in  $^{16}\text{N}$  were measured using a high-precision Q3D magnetic spectrograph. The neutron spectroscopic factors and the asymptotic normalization coefficients for these states in  $^{16}\text{N}$  were then derived based on distorted wave Born approximation analysis. The proton widths of the four low-lying resonant states in  $^{16}\text{F}$  were obtained according to charge symmetry of strong interaction.

PACS numbers: 25.60.Je; 21.10.Jx; 21.10.Tg; 27.20.+n

---

\*Corresponding author: guobing@ciae.ac.cn

## I. INTRODUCTION

In the past there has been considerable effort to explore the structure of  $^{16}\text{N}$ , while there is fewer report for its mirror analog  $^{16}\text{F}$  since it can be investigated through relatively few reactions including  $^{14}\text{N}(^3\text{He}, n)^{16}\text{F}$  [1–3],  $^{16}\text{O}(p, n)^{16}\text{F}$  [4–8],  $^{16}\text{O}(^3\text{He}, t)^{16}\text{F}$  [9–12], and  $^{19}\text{F}(^3\text{He}, ^6\text{He})^{16}\text{F}$  [10]. The level diagram for the four low-lying states in mirror pair of  $^{16}\text{N}$ - $^{16}\text{F}$  is shown in Fig. 1. All the states in  $^{16}\text{F}$  are unbound and decay as  $^{15}\text{O} + p$ . The measurements using stable beams have well determined spin-parity values and excitation energies with an accuracy of 4-6 keV for the four low-lying states in  $^{16}\text{F}$  [13]. However, these measurements yielded only upper limits or rough estimates of the  $^{16}\text{F}$  level widths. Recently, Lee et al. investigated the level widths of these four states in  $^{16}\text{F}$  via the elastic resonance scattering of  $^{15}\text{O} + p$  based on a thick target inverse kinematics method [14]. Although these authors significantly improved values for these level widths of  $^{16}\text{F}$ , it is still desirable to perform a new measurement of these level widths via an independent approach.

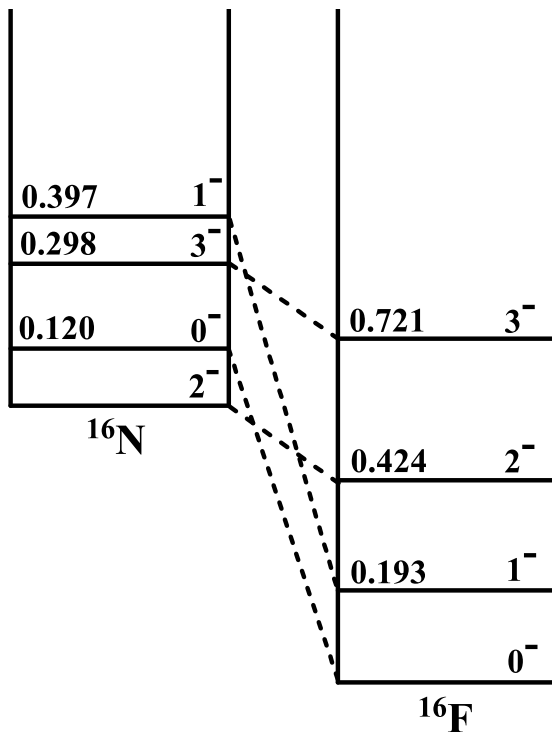


FIG. 1: Level diagram for the low-lying states in mirror pair of  $^{16}\text{N}$ - $^{16}\text{F}$ .

In the present work, we measure the angular distributions of the  $^{15}\text{N}(^7\text{Li}, ^6\text{Li})^{16}\text{N}$  reaction populating the four low-lying states in  $^{16}\text{N}$ . The neutron spectroscopic factors and the

asymptotic normalization coefficients (ANCs) for these states are then derived based on distorted wave Born approximation (DWBA) analysis. The proton widths of the four low-lying resonant states in the mirror analog  $^{16}\text{F}$  are extracted according to charge symmetry of mirror nuclei. Similar approach has been successfully used to study many mirror pairs such as  $^{12}\text{B}$ - $^{12}\text{N}$  [15],  $^{15}\text{C}$ - $^{15}\text{F}$  [16],  $^{27}\text{Mg}$ - $^{27}\text{P}$  [17] and  $^{57}\text{Ni}$ - $^{57}\text{Cu}$  [18]. Most recently, a short paper concerning the  $^{15}\text{N}(^7\text{Li}, ^6\text{Li})^{16}\text{N}$  angular distributions and determination of the astrophysical  $^{15}\text{N}(n, \gamma)^{16}\text{N}$  reaction rate has been published elsewhere [19].

## II. EXPERIMENTAL PROCEDURE

The measurement of the angular distributions was performed at the HI-13 tandem accelerator of the China Institute of Atomic Energy (CIAE) in Beijing. The experimental setup and procedures are similar to those reported previously [20–22]. A  $^7\text{Li}$  beam with an energy of 44 MeV was used to measure the angular distributions of the  $^{15}\text{N}(^7\text{Li}, ^6\text{Li})^{16}\text{N}$  reaction populating the ground state and the first three excited states at  $E_x = 0.120$ , 0.298, and 0.397 MeV in  $^{16}\text{N}$ . In addition, the angular distribution of the  $^7\text{Li} + ^{15}\text{N}$  elastic scattering was measured to obtain the optical model potential (OMP) parameters for the entrance channel of the transfer reaction. To extract the exit channel OMP parameters a 34.5 MeV  $^6\text{Li}$  beam was also delivered for the measurement of the angular distribution for the  $^6\text{Li} + ^{15}\text{N}$  elastic scattering.

Melamine  $\text{C}_3\text{N}_3(^{15}\text{NH}_2)_3$  enriched to 99.35% in  $^{15}\text{N}$  was employed as target material with a thickness of  $46 \mu\text{g}/\text{cm}^2$ , which was evaporated on a  $30 \mu\text{g}/\text{cm}^2$  thick carbon foil. In addition, a  $^{14}\text{N}$  target was used for background evaluation. To improve the thermal conductivity of the targets a  $22 \mu\text{g}/\text{cm}^2$  thick gold was evaporated on melamine foil. The target thickness was determined using an analytical balance with a precision of  $1 \mu\text{g}$  and was verified with the well-known differential cross sections of the  $^7\text{Li} + ^{15}\text{N}$  elastic scattering at  $\theta_{\text{c.m.}} = 33.5^\circ$  and  $49.2^\circ$  [23, 24]. After considering the balance precision and the error of the differential cross sections, an uncertainty of 5% was assigned for target thickness.

A movable Faraday cup covering an angular range of  $\pm 6^\circ$  in laboratory frame was used to measure the beam current for normalization of the cross sections at  $\theta_{\text{lab}} > 6^\circ$ . The Faraday cup was removed when measuring the cross sections at  $\theta_{\text{lab}} \leq 6^\circ$ . A silicon  $\Delta E - E$  telescope located at  $\theta_{\text{lab}} = 25^\circ$  was employed for normalization of the cross sections at

$\theta_{\text{lab}} \leq 6^\circ$  by measuring the elastic scattering of the incident ions on the targets. The reaction products were analyzed with a Q3D magnetic spectrograph and were recorded by a two-dimensional position-sensitive silicon detector (PSSD,  $50 \times 50$  mm) placed at the focal plane of the spectrograph. The two-dimensional position information from the PSSD enabled the products emitted into the acceptable solid angle to be recorded completely. The energy information from the PSSD was used to remove the impurities with the same magnetic rigidity.

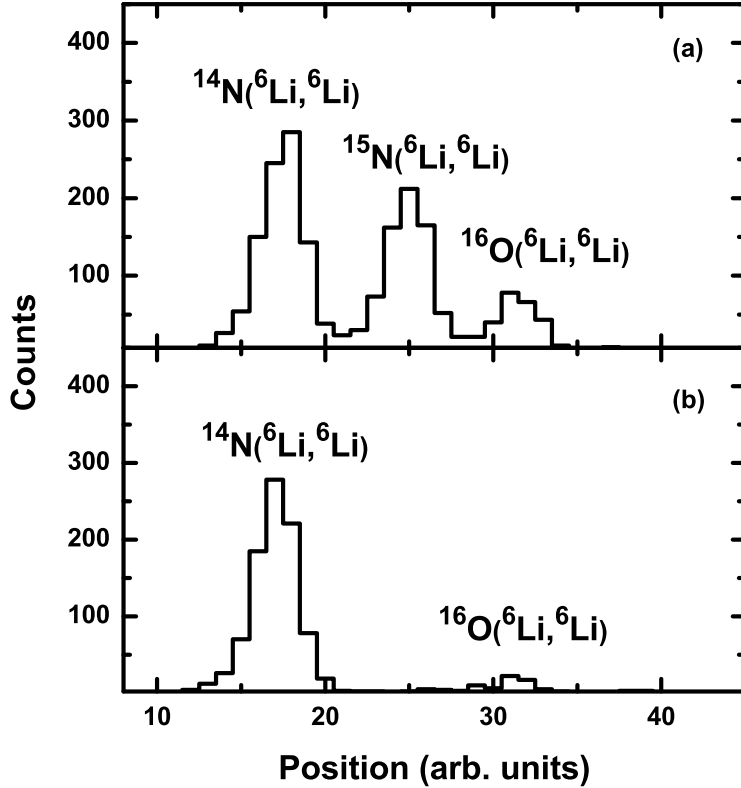


FIG. 2: Focal-plane position spectra of the  ${}^6\text{Li}$  events at  $\theta_{\text{lab}} = 18^\circ$  from the elastic scattering on the enriched  ${}^{15}\text{N}$  target (a) and the natural  ${}^{14}\text{N}$  target (b).

As an example, Figure 2 displays the focal-plane position spectra of the  ${}^6\text{Li}$  events at  $\theta_{\text{lab}} = 18^\circ$  from the elastic scattering on the enriched  ${}^{15}\text{N}$  target and the natural  ${}^{14}\text{N}$  target. One sees that the events from the elastic scattering on different isotopes in the targets can be clearly separated. The events from the elastic scattering on carbon and gold ran out of the PSSD due to larger energy differences. It should be mentioned that the elastic scattering events from  ${}^{15}\text{N}$  and  ${}^{14}\text{N}$  cannot be separated any more when measuring the cross sections at

$\theta_{\text{lab}} < 15^\circ$ . This is because the energy difference of  ${}^6\text{Li}$  from the elastic scattering on different isotopes decreases with  $\theta_{\text{lab}}$ . Therefore, the background from  ${}^{14}\text{N}$  needs to be evaluated to obtain the cross sections at  $\theta_{\text{lab}} < 15^\circ$ . The angular distributions of the elastic scattering were obtained after background subtraction and beam normalization, as shown in Fig. 3.

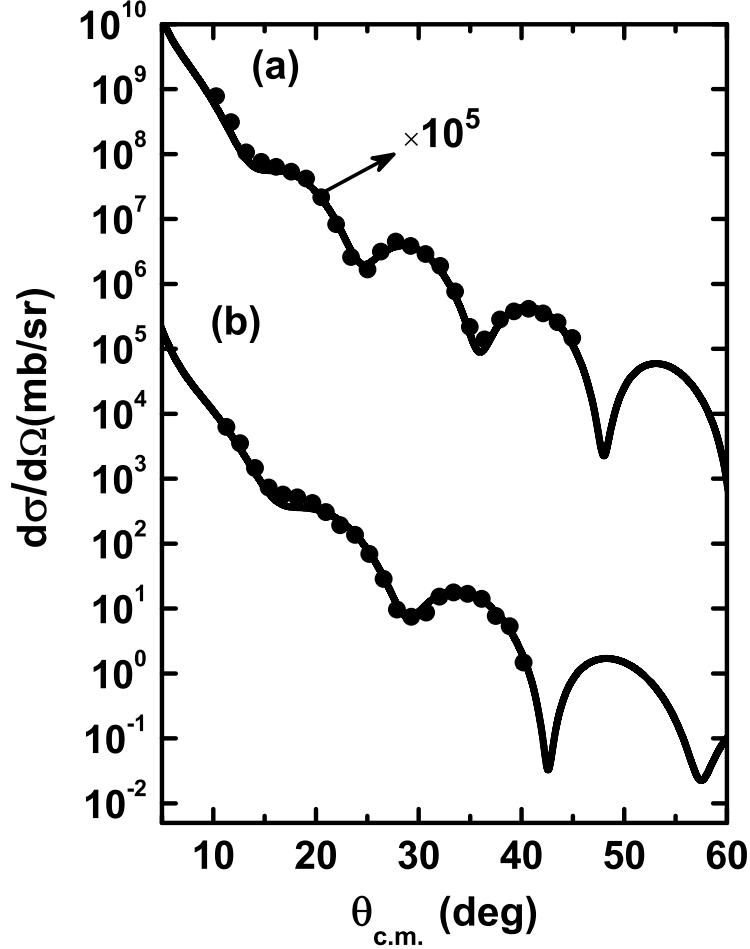


FIG. 3: Angular distributions of the  ${}^7\text{Li}+{}^{15}\text{N}$  elastic scattering at incident energy of 44 MeV (a) and the  ${}^6\text{Li}+{}^{15}\text{N}$  elastic scattering at incident energy of 34.5 MeV (b). The solid curves represent the calculations with the fitted OMP parameters.

In Fig. 4 we display the focal-plane position spectrum of  ${}^6\text{Li}$  at  $\theta_{\text{lab}} = 10^\circ$  from the  ${}^{15}\text{N}({}^7\text{Li}, {}^6\text{Li}){}^{16}\text{N}$  reaction leading to the ground state and the first three excited states at  $E_x = 0.120, 0.298, \text{ and } 0.397$  MeV in  ${}^{16}\text{N}$ . The closely spaced levels in  ${}^{16}\text{N}$  were resolved and the background from  ${}^{14}\text{N}$  is negligibly small. After background subtraction and beam normalization, the angular distributions of the  ${}^{15}\text{N}({}^7\text{Li}, {}^6\text{Li}){}^{16}\text{N}$  reaction were obtained, as presented in Fig. 5.

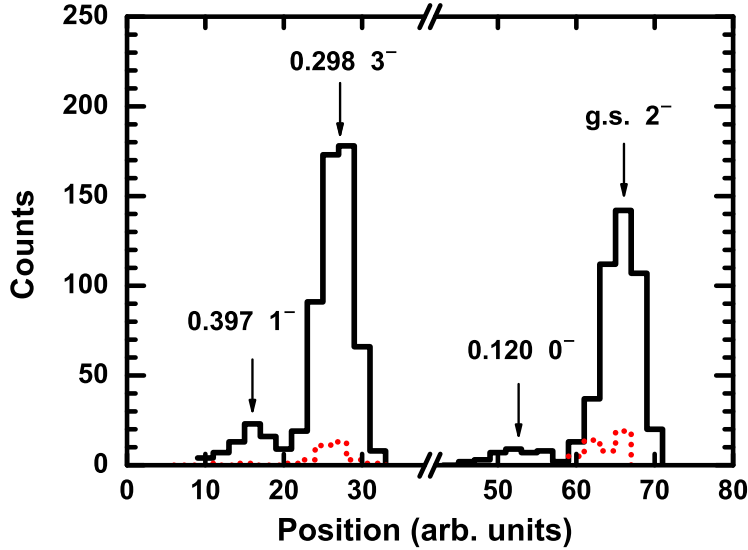


FIG. 4: (Color online) Focal-plane position spectrum of the  ${}^6\text{Li}$  events at  $\theta_{\text{lab}} = 10^\circ$  from the  ${}^{15}\text{N}({}^7\text{Li}, {}^6\text{Li}){}^{16}\text{N}$  reaction. The black solid and red dashed lines denote the results from the enriched  ${}^{15}\text{N}$  target and the natural  ${}^{14}\text{N}$  target, respectively. The break in the x-axis denotes the narrow gap between two separated detectors.

### III. SPECTROSCOPIC FACTORS OF THE LOW-LYING STATES IN ${}^{16}\text{F}$

The experimental angular distributions were analyzed with the finite-range DWBA code FRESKO [25]. The OMP parameters for the entrance and exit channels were extracted by fitting the present experimental angular distributions of the  ${}^7\text{Li} + {}^{15}\text{N}$  and  ${}^6\text{Li} + {}^{15}\text{N}$  elastic scattering (Fig. 3). The starting values of the OMP parameters were obtained by fitting the systematic nucleus-nucleus potential based on a single-folding model [26]. The real potential was chosen as a squared Woods-Saxon form, which fits the real part of the folding model potential better than the usual Woods-Saxon form does [27]. For the imaginary potential the usual Woods-Saxon form was found to be appropriate. In addition, we investigated the effect of spin-orbit potential parameters although for heavy ions they are thought to have little or no influence on the cross sections [28]. Full complex remnant term interactions were included in the transfer reaction calculations. The core-core ( ${}^6\text{Li} + {}^{15}\text{N}$ ) potential parameters were determined using the present ones of  ${}^6\text{Li} + {}^{15}\text{N}$  at 34.5 MeV and the systematics in energy dependence of the potential parameters of Ref. [26]. For the wave function of bound states, the Woods-Saxon potential with the standard geometric parameters ( $r = 1.25$  fm

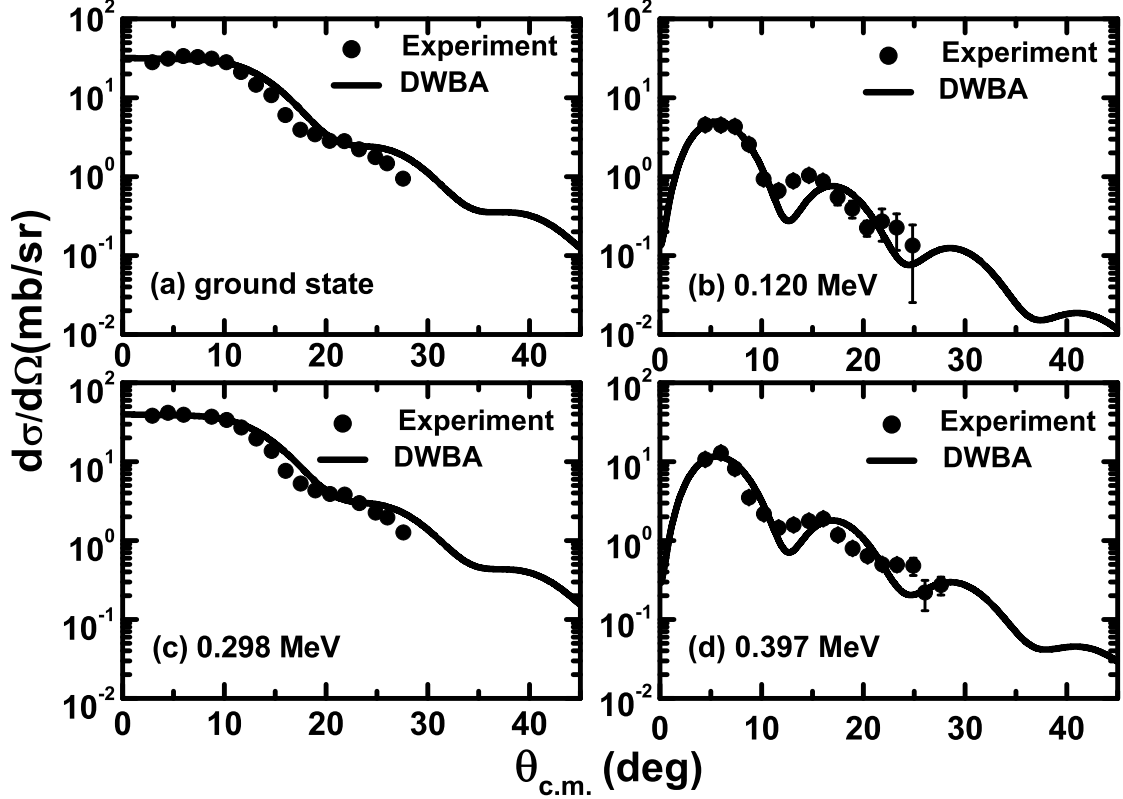


FIG. 5: Angular distributions of the  $^{15}\text{N}(^7\text{Li}, ^6\text{Li})^{16}\text{N}$  reaction leading to the ground and first three excited states in  $^{16}\text{N}$ . The curves represent the DWBA calculations with the fitted OMP parameters.

and  $a = 0.65$  fm) was adopted, which have been extensively utilized to study the ground state neutron spectroscopic factors for 80 nuclei of  $Z = 3-24$  [29] and 565 excited state neutron spectroscopic factors for  $Z = 8-28$  nuclei [30]. The potential depths were adjusted to reproduce the neutron binding energies. All the parameters are listed in Table I.

The spectroscopic factors of  $^{16}\text{N}$  can be derived by the comparison of the experimental angular distribution with the DWBA calculations using the relationship,

$$\sigma_{l,j}^{\text{exp}}(\theta) = S_{l,j}^{16\text{N}} [S_{1,3/2}^{7\text{Li}} \sigma_{1,3/2}^{\text{DW}}(\theta) + S_{1,1/2}^{7\text{Li}} \sigma_{1,1/2}^{\text{DW}}(\theta)]. \quad (1)$$

Here  $S_{l,j}^{16\text{N}}$  is the spectroscopic factor of  $^{16}\text{N}$ .  $S_{1,3/2}^{7\text{Li}}$  and  $S_{1,1/2}^{7\text{Li}}$  are the spectroscopic factors of  $^7\text{Li}$ , corresponding to the  $j = 3/2$  and  $j = 1/2$  orbits. The square of the ANC's for the virtual decay  $^{16}\text{N} \rightarrow ^{15}\text{N} + n$  was determined through  $(C_{l,j}^{16\text{N}})^2 = S_{l,j}^{16\text{N}} \times (b_{l,j}^{16\text{N}})^2$ , where  $b_{l,j}^{16\text{N}}$  is the single-particle ANC of the bound state neutron in  $^{16}\text{N}$ .



TABLE I: OMP parameters used in the present DWBA calculation.  $E_{\text{in}}$  denotes the incident energy in MeV for the relevant channels,  $V$  and  $W$  are the depths (in MeV) of the real and imaginary potentials with the squared Woods-Saxon form and the usual Woods-Saxon form, and  $r$  and  $a$  are the radius and the diffuseness (in fm).  $\chi_\nu^2$  is the reduced chi-square for the fitting.

Channel	$E_{\text{in}}$	$V$	$r_v$	$a_v$	$W$	$r_w$	$a_w$	$V_{so}$	$r_{so}$	$a_{so}$	$r_C$	$\chi_\nu^2$
${}^7\text{Li}+{}^{15}\text{N}$	44.0	138.7	0.911	1.26	45.0	0.966	0.820				1.30	4.08
${}^6\text{Li}+{}^{16}\text{N}$	34.5	111.0	0.886	1.47	39.0	0.840	1.02				1.30	3.98
${}^6\text{Li}+{}^{15}\text{N}$	37.7	132.0	0.901	1.37	31.3	0.945	0.918				1.30	
$n+{}^{15}\text{N}$		<sup>a</sup>	1.25	0.65				6.0	1.25	0.65	1.25	

<sup>a</sup>The depth was obtained by fitting to reproduce the binding energy of the neutron in  ${}^{16}\text{N}$ .

To study  $S_{l,j}^{16\text{N}}$ ,  $S_{1,3/2}^{7\text{Li}}$  and  $S_{1,1/2}^{7\text{Li}}$  need to be determined. The value of 0.73 was chosen as the total neutron spectroscopic factor ( $S_{1,3/2}^{7\text{Li}} + S_{1,1/2}^{7\text{Li}}$ ) of the  ${}^7\text{Li}$  ground state [31–34], as stated in Ref. [19]. According to the shell model calculation [31], the ratio of  $S_{1,3/2}^{7\text{Li}}$  to  $S_{1,1/2}^{7\text{Li}}$  was derived to be 1.5. The spectroscopic factors of the ground state and the first three excited states in  ${}^{16}\text{N}$  were then extracted to be  $0.96 \pm 0.09$ ,  $0.69 \pm 0.09$ ,  $0.84 \pm 0.08$  and  $0.65 \pm 0.08$ , respectively. The errors result from the statistics (8%, 12%, 8%, 11%), the uncertainty of target thickness (5%) and the uncertainty of spin-orbit potential parameters (1.6%, 2.2%, 1.2%, 3.1%), respectively. The present spectroscopic factors are approximately two times larger than those from the  ${}^{15}\text{N}(d, p)$  reaction [35], while they are in good agreement with those from the  ${}^2\text{H}({}^{15}\text{N}, p)$  reaction using Method2 (namely, components allowed to vary freely) in Ref. [36] where two different methods were used to determine the spectroscopic factors since the closely spaced levels (ground state + 0.120 MeV level, 0.298 + 0.397 MeV levels) in  ${}^{16}\text{N}$  could not be resolved. It should be mentioned that the relative spectroscopic factor values from all three measurements agree within uncertainties. In addition, the squares of the ANCs for the virtual decay  ${}^{16}\text{N} \rightarrow {}^{15}\text{N} + n$  were derived to be  $0.188 \pm 0.018$ ,  $3.54 \pm 0.46$ ,  $0.128 \pm 0.012$  and  $2.81 \pm 0.36 \text{ fm}^{-1}$ , respectively. All these results are listed in Table II.

We also investigated the dependence of the ANCs on the geometric parameters of the Woods-Saxon potential for the single-particle bound state in  ${}^{16}\text{N}$ . In the present calculation the radius was adjusted and the new well depth was readjusted to reproduce the binding energy. The result shows that for two levels corresponding to neutron transfers to the  $1d_{5/2}$

TABLE II: Present spectroscopic factors of  $^{16}\text{N}$  and the square of the ANCs for the virtual decay  $^{16}\text{N} \rightarrow ^{15}\text{N} + n$ .  $nl_j$  is the single-particle shell quantum number.

$E_x$ (MeV)	$J^\pi$	$nl_j$	$S_{l,j}^{16\text{N}}$	$(C_{l,j}^{16\text{N}})^2$ ( $\text{fm}^{-1}$ )
0	$2^-$	$1d_{5/2}$	$0.96 \pm 0.09$	$0.188 \pm 0.018$
0.120	$0^-$	$2s_{1/2}$	$0.69 \pm 0.09$	$3.54 \pm 0.46$
0.298	$3^-$	$1d_{5/2}$	$0.84 \pm 0.08$	$0.128 \pm 0.012$
0.397	$1^-$	$2s_{1/2}$	$0.65 \pm 0.08$	$2.81 \pm 0.36$

orbit the spectroscopic factors vary significantly, while the ANCs are nearly constant. This indicates that the ANCs for these two levels are model independent. Contrarily, the ANCs vary almost as significantly as the spectroscopic factors do for two levels corresponding to neutron transfers to the  $2s_{1/2}$  orbit, which indicates that the ANCs for these two levels are model dependent. This difference in response to transfers to the  $1d_{5/2}$  and  $2s_{1/2}$  states may stem from the different peripheralities of these two transitions.

#### IV. PROTON WIDTHS OF THE LOW-LYING RESONANT STATES IN $^{16}\text{F}$

The width  $\Gamma_p$  of a proton resonance can be calculated through

$$\Gamma_p = S_{l,j}^{16\text{F}} \times \Gamma_p^{s.p.}, \quad (2)$$

where  $\Gamma_p^{s.p.}$  denotes the single-particle width which can be calculated from the scattering phase shift in a Woods-Saxon potential. We assume that the spectroscopic factors for mirror pair are equal ( $S_{l,j}^{16\text{F}} = S_{l,j}^{16\text{N}}$ ) according to charge symmetry of strong interaction, thus the  $\Gamma_p$  of  $^{16}\text{F}$  can be derived from the spectroscopic factors of  $^{16}\text{N}$  via Eq. 2.

We studied the dependence of the proton widths of  $^{16}\text{F}$  ( $\Gamma_p$ ), the spectroscopic factors ( $S_{l,j}^{16\text{F}}$ ), and the single-particle width ( $\Gamma_p^{s.p.}$ ) on the geometric parameter by changing the radius ( $R = r \cdot A^{1/3}$ ) within a reasonable range from 2.6 to 3.6 fm. The  $^{16}\text{F}$  spectroscopic factors are equal to the  $^{16}\text{N}$  ones which were obtained using the new depths readjusted to match the binding energies of the neutron in  $^{16}\text{N}$ . The single-particle widths were computed with the new depths determined by fitting to reproduce the resonance energies of the proton in  $^{16}\text{F}$ . As shown in Fig. 6, the single-particle widths and the spectroscopic factors of  $^{16}\text{F}$  vary significantly, while the proton widths are nearly constant. This indicates that the proton

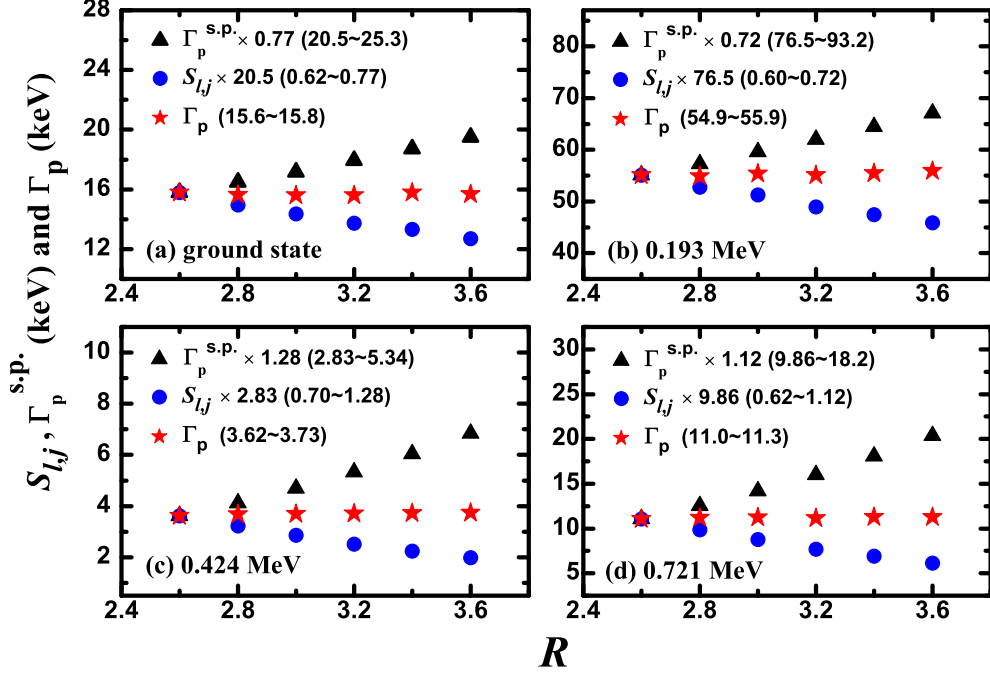


FIG. 6: (Color online) Dependence of the single-particle width ( $\Gamma_p^{s.p.}$ ), the spectroscopic factors of  $^{16}\text{F}$  ( $S_{l,j}^{16\text{F}}$ ), and the proton widths of  $^{16}\text{F}$  ( $\Gamma_p$ ) on the radius ( $R$ ). (a)-(d) represent the results for the ground state and the first three excited states in  $^{16}\text{F}$ , respectively.  $\Gamma_p^{s.p.}$  and  $S_{l,j}$  are normalized to the  $\Gamma_p$  value at  $R = 2.6$  fm. The ranges in the present results are given in parentheses.

widths of the four  $^{16}\text{F}$  states are model independent. The proton widths were derived to be  $15.7 \pm 2.0$ ,  $55.3 \pm 7.2$ ,  $3.66 \pm 0.35$ , and  $11.2 \pm 1.1$  keV for these four states using the average values for different radius, as listed in Table III. The uncertainties of geometric parameters were determined by taking the half difference between the maximum and minimum widths in Fig. 6. They were found to be less than 1.5% for all four levels in  $^{16}\text{F}$ , thus the error of the present proton widths mainly results from the uncertainty of the spectroscopic factors.

In Table IV we compare different evaluations of the proton widths from the present work and the previous studies. The present width of the  $^{16}\text{F}$  ground state is narrower than the lower limits from the compilation [13] and the  $^{14}\text{N}(^3\text{He}, n)$  data [1, 3], and is narrower than the value from the  $^{16}\text{O}(^3\text{He}, t)$  data [11]. The new width of the first excited state is larger than the upper limits of Refs. [1, 13], while is narrower than those of Refs. [3, 11, 12]. The present width of the second excited state is narrower than the lower limits from the compilation [13] and the  $^{14}\text{N}(^3\text{He}, n)$  data [1, 3]. In addition, our results are in good agreement with those

TABLE III: The spectroscopic factors ( $S_{l,j}^{16\text{F}}$ ), the single-particle width ( $\Gamma_p^{s.p.}$ ), and the proton widths of  $^{16}\text{F}$  ( $\Gamma_p$ ).  $S_{l,j}^{16\text{F}}$  and  $\Gamma_p^{s.p.}$  are obtained with standard geometric parameters, while  $\Gamma_p$  are the average values for the radius range from  $R = 2.6$  to  $3.6$  fm

$E_x(\text{MeV})$	$J^\pi$	$nl_j$	$S_{l,j}^{16\text{F}}$	$\Gamma_p^{s.p.}$ (keV)	$\Gamma_p$ (keV)
0.000	$0^-$	$2s_{1/2}$	$0.69 \pm 0.09$	22.7	$15.7 \pm 2.0$
0.193	$1^-$	$2s_{1/2}$	$0.65 \pm 0.08$	84.1	$55.3 \pm 7.2$
0.424	$2^-$	$1d_{5/2}$	$0.96 \pm 0.09$	3.86	$3.66 \pm 0.35$
0.721	$3^-$	$1d_{5/2}$	$0.84 \pm 0.08$	13.3	$11.2 \pm 1.1$

TABLE IV: Present  $^{16}\text{F}$  proton widths in keV and other available results in the literature.

$E_x$ (MeV)	Compilation [13]	$^{14}\text{N}(^3\text{He}, n)$ [1]	$^{14}\text{N}(^3\text{He}, np)$ [3]	$^{16}\text{O}(^3\text{He}, t)$ [11]	$^{16}\text{O}(^3\text{He}, t)$ [12]	$p(^{15}\text{O}, p)$ [14]	$^{15}\text{N}(^7\text{Li}, ^6\text{Li})$ Present
0.000	$40 \pm 20$	$50 \pm 30$	$39 \pm 20$	$\approx 25$	$18 \pm 16$	$22.8 \pm 7.2$	$15.7 \pm 2.0$
0.193	$< 40$	$< 40$	$96 \pm 20$	$\approx 100$	$87 \pm 16$	$103 \pm 6$	$55.3 \pm 7.2$
0.424	$40 \pm 30$	$40 \pm 30$	$24 \pm 20$		$16 \pm 16$	$4.0 \pm 1.3$	$3.66 \pm 0.35$
0.721	$< 15$	$< 15$	$24 \pm 20$		$12 \pm 16$	$15.1 \pm 3.4$	$11.2 \pm 1.1$

from the most recent  $p(^{15}\text{O}, p)$  data [14] for all the levels except the first excited state. The width of  $103 \pm 9$  keV for the first excited state given in Ref. [14] would yield a spectroscopic factor of  $1.22 \pm 0.11$ , which is significantly larger than the present result ( $0.65 \pm 0.08$ ) from the  $^{15}\text{N}(^7\text{Li}, ^6\text{Li})^{16}\text{N}$  data and that ( $0.74 \pm 0.12$ ) from the  $^{15}\text{N}(d, p)^{16}\text{N}$  data [36] and the shell model prediction (0.96) [37]. Therefore, additional measurements of this width via an independent method are certainly desirable.

## V. DISCUSSION AND CONCLUSION

The angular distributions of the  $^{15}\text{N}(^7\text{Li}, ^6\text{Li})^{16}\text{N}$  reaction were measured by a high-precision Q3D magnetic spectrograph and were utilized to determine the neutron spectroscopic factors and the ANCs for the four low-lying  $^{16}\text{N}$  states. We also investigated the dependence of our results on the geometric parameters of the Woods-Saxon potential for

the single-particle bound state in  $^{16}\text{N}$ . It was found that the ANCs for the two levels corresponding to neutron transfers to the  $1d_{5/2}$  orbit are more model independent than the ANCs for the two levels corresponding to neutron transfers to the  $2s_{1/2}$  orbit. This difference may come from the different peripheralities of these two transitions.

The proton widths of the four low-lying levels in  $^{16}\text{F}$  were determined from the  $^{16}\text{N}$  spectroscopic factors by charge symmetry of mirror nuclei. In addition, we studied the dependence of the proton widths on the geometric parameters of the Woods-Saxon potential. The result demonstrates that the proton widths of these four states in  $^{16}\text{F}$  are all model independent. The new widths are in good agreement with those from the most recent  $p(^{15}\text{O}, p)$  data [14] for the ground state, the second and third excited states in  $^{16}\text{F}$ . For the first excited state the present width is nearly half of that in Ref. [14]. To understand this discrepancy additional measurements of this width via an independent method are highly desirable.

### Acknowledgments

We acknowledge the staff of HI-13 tandem accelerator for the smooth operation of the machine, and N. K. Timofeyuk and R. C. Johnson for their helpful discussions on DWBA calculations and charge symmetry. This work was performed with the support of the National Natural Science Foundation of China under Grant Nos. 11321064, 11075219, 11375269, 11275272 and 11275018, the 973 program of China under Grant No. 2013CB834406.

- 
- [1] C. D. Zafiratos, F. Ajzenberg-Selove and F. S. Dietrich, Phys. Rev. **137**, B1479 (1965).
  - [2] W. Bohne, H. Fuchs, K. Grabisch et al., Phys. Lett. B **47**, 342 (1973).
  - [3] T. Otsubo, I. Asada, M. Takeda et al., Nucl. Phys. A **259**, 452 (1976).
  - [4] C. E. Moss and A. B. Comiter, Nucl. Phys. A **178**, 241 (1971).
  - [5] A. Fazely, B. D. Anderson, M. Ahmad et al., Phys. Rev. C **25**, 1760 (1982).
  - [6] H. Orihara, S. Nishihara, K. Furukawa et al., Phys. Rev. Lett. **49**, 1318 (1982).
  - [7] H. Ohnuma, M. Kabasawa, K. Furukawa et al., Nucl. Phys. A **467**, 61 (1987).
  - [8] R. Madey, B. S. Flanders, B. D. Anderson et al., Phys. Rev. C **56**, 3210 (1997).
  - [9] R. H. Pehl and J. Cerny, Phys. Lett. **14**, 137 (1965).

- [10] H. Nann, W. Benenson, E. Kashy, H. P. Morsch and D. Mueller, *Phys. Rev. C* **16**, 1684 (1977).
- [11] W. A. Sterrenburg, S. Brandenburg, J. H. Van Dijk et al., *Nucl. Phys. A* **420**, 257 (1984).
- [12] H. Fujita, G. P. A. Berg, Y. Fujita et al., *Phys. Rev. C* **79**, 024314 (2009).
- [13] D. R. Tilley, H. R. Weller and C. M. Cheves, *Nucl. Phys. A* **564**, 1 (1993).
- [14] D. W. Lee, K. Peräjärvi, J. Powell et al., *Phys. Rev. C* **76**, 024314 (2007).
- [15] B. Guo, Z. H. Li, W. P. Liu et al., *J. Phys. G* **34**, 103 (2007).
- [16] N. K. Timofeyuk, D. Baye, P. Descouvemont, R. Kamouni and I. J. Thompson, *Phys. Rev. Lett.* **96**, 162501 (2006).
- [17] B. Guo, Z. H. Li, X. X. Bai et al., *Phys. Rev. C* **73**, 048801 (2006).
- [18] K. E. Rehm, F. Borasi, C. L. Jiang et al., *Phys. Rev. Lett.* **80**, 676 (1998).
- [19] B. Guo, Z. H. Li, Y. J. Li et al., *Phys. Rev. C* **89**, 012801(R) (2014).
- [20] B. Guo, Z. H. Li, M. Lugaro et al., *Astrophys. J.* **756**, 193 (2012).
- [21] Y. J. Li, Z. H. Li, E. T. Li et al., *Eur. Phys. J. A* **48**, 13 (2012).
- [22] Z. H. Li, Y. J. Li, J. Su et al., *Phys. Rev. C* **87**, 017601 (2013).
- [23] C. L. Woods, B. A. Brown and N. A. Jelley, *J. Phys. G* **8**, 1699 (1982).
- [24] F. de Oliveira, A. Coc, P. Aguer et al., *Nucl. Phys. A* **597**, 231 (1996).
- [25] I. J. Thompson, *Comput. Phys. Rep.* **7**, 167 (1988).
- [26] Y. P. Xu and D. Y. Pang, *Phys. Rev. C* **87**, 044605 (2013).
- [27] D. T. Khoa, W. V. Oertzen, H. G. Bohlen and S. Ohkubo, *J. Phys. G* **34**, R111 (2007).
- [28] L. Trache, A. Azhari, H. L. Clark et al., *Phys. Rev. C* **61**, 024612 (2000).
- [29] M. B. Tsang, J. Lee and W. G. Lynch, *Phys. Rev. Lett.* **95**, 222501 (2005).
- [30] M. B. Tsang, J. Lee, S. C. Su et al., *Phys. Rev. Lett.* **102**, 062501 (2009).
- [31] S. Cohen and D. Kurath, *Nucl. Phys. A* **101**, 1 (1967).
- [32] T. Y. Li and S. K. Mark, *Nucl. Phys. A* **123**, 147 (1969).
- [33] I. S. Towner, *Nucl. Phys. A* **126**, 97 (1969).
- [34] J. Su, Z. H. Li, B. Guo et al., *Chin. Phys. Lett.* **27**, 052101 (2010).
- [35] W. Bohne, J. Bommer, H. Fuchs et al., *Nucl. Phys. A* **196**, 41 (1972).
- [36] D. W. Bardayan, P. D. O'Malley, J. C. Blackmon et al., *Phys. Rev. C* **78**, 052801(R) (2008).
- [37] J. Meissner, H. Schatz, H. Herndl et al., *Phys. Rev. C* **53**, 977 (1996).